Assessment of an evolution equation for the averaged displacement speed of a reactive scalar field

ASSESSMENT OF AN EVOLUTION EQUATION FOR THE AVERAGED DISPLACEMENT SPEED OF A REACTIVE SCALAR FIELD

Rixin Yu*, Thommie Nilsson*, Xue-Song Bai*, Andrei N. Lipatiknov**
rixin.yu@energy.lth.se
*Div. Fluid Mechanics, Dept. of Energy Sciences, Lund University, 22100 Lund, Sweden
**Department of Mechanics and Maritime Sciences, Chalmers University of Technology, Göteborg, 412 96, Sweden

Abstract
For turbulent premixed reacting flow modeled by a simplified transport equation for a reaction progress scalar field, an evolution equation for the displacement speed conditionally averaged on the reaction progress was derived in a recent work. In the current paper this equation is used to analyze the basic problem of propagation of a planar reaction wave in homogeneous isotropic constant-density turbulence using a DNS approach. We examine both the transient process of the initial planar wave being disturbed by turbulence as well as the fully developed wave after all statistics has evolved to a stationary state. The numerical results support the derived equation by showing good match between the left hand side term and the sum of all right hand side terms. The derived equation reveals three effects that cause temporal variation in averaged displacement speed: (i) T_1, the isosurface-following rate of change in reaction surface density, (ii) T_2, the isosurface-following rate of change due to diffusion, and (iii) T_3, a stretch-rate-induced difference between averaged isosurface-following derivative and time derivative of the isosurface averaged value. For a fully developed wave the equation reduces to a constraint of zero sum of the three terms; this is realized by (i) the terms T_1 and T_3 averaged over all reaction scalar zones stay positive and negative, respectively, and (ii) T_2 stays largely positive except in the preheat zone for a highly disturbed reaction wave where it becomes slightly negative. Among the three terms, the diffusion contribution term T_3 is found to be largely responsible for early transient variation in averaged displacement speed. For the transient evolution of highly turbulent reaction waves, it is also found that all three terms tend to flip their signs when moving from the preheat zone to the reaction zone.

Introduction

A turbulent premixed flame is often modeled using a reaction progress variable c which is zero and unity on the side of unburned fresh reactant and burned product, respectively. The evolution of c is described by the convection-diffusion-reaction equation

$$\frac{\partial c}{\partial t} + \boldsymbol{u} \cdot \nabla c = \mathbb{D} + \mathbb{W}, \tag{1}$$

where t, $\boldsymbol{u}$, $\mathbb{D}$, and $\mathbb{W}$ denote time, flow velocity vector, diffusion term, and the reaction rate term, respectively. One quantity of particular interest is the displacement speed S_d of the scalar field c relative to the local fluid. The displacement speed is controlled by the combined effect of diffusion and reaction and is defined as

$$S_d \equiv (\mathbb{D} + \mathbb{W})/|\nabla c|. \tag{2}$$

In a turbulent reacting flow the displacement speed is defined for any point $(\boldsymbol{x}, t)$ for which

$0 < c(\boldsymbol{x}, t) < 1$. The displacement speed contains information that characterize the self-propagation of the local reaction wave. Knowing statistical information on the displacement speed can benefit premixed combustion modeling based for example on the level-set (G-equation) formulation [1] or the flame surface density approach for reaction rate closure [2]. Furthermore, the variation of displacement speed across different zones inside the reaction wave can tell about changes in the internal wave structure induced by turbulence and such information can be particularly useful when studying heavily disturbed flames characterized by a large Karlovitz number (Ka).

Statistical behavior of the displacement speed has been the topic of a number of studies based on direct numerical simulations (DNS) of various turbulent reacting flows, see [3–6] and references therein. In the literature the displacement speed is often examined by correlating with other quantities characterizing turbulent reacting flow, including local curvature, surface topology, strain rate and alignment characteristics of scalar gradient with principle strain rates. It is also common to decompose the displacement speed into three component contributions due to reaction, diffusion in the normal direction, and diffusion induced by curvature. Particular focus has been put on the probability of finding locally negative displacement speed as well as the sign of the averaged displacement speed. While previous studies that rely on comparing relations in quantities extracted from DNS data do show the potential to contribute to the understanding of turbulence/flame interactions, the mechanism governing the dynamic evolution of displacement speed is still not well understood. This may be attributed to the lack of a quantitative framework describing the evolution of displacement speed that advanced analyses may rely on.

To better understand the self propagation of turbulent reaction waves characterized by the displacement speed, we derived in a recent paper [7] a new evolution equation for S_d conditionally averaged on the reaction progress variable for a simplified reaction wave. Using this equation, Eq. (10) shown below, the temporal evolution of the averaged displacement speed can be attributed to the right hand side (rhs) terms representing different physical effects. Each term in this equation can be numerically extracted from DNS. It was demonstrated in [7] using several DNS cases that the left hand side (lhs) term match well with the sum of all rhs terms even for a highly turbulent case with a Karlovitz number of 390.

The previous paper [7] focused on theoretical aspects of the equation derivation and examination of the equation after the turbulent reaction wave has developed to statistical stationarity. In this work we study the physical interpretation of the equation terms as well as the transient non-equilibrium behavior.

Evolution equation for averaged displacement speed

This section gives a very brief description of the derivation the evolution equation for surface-averaged displacement speed. More details can be found in [7].

For an arbitrary quantity $\phi(\boldsymbol{x}, t)$ an isosurface-following time derivative operator $\partial^*/\partial^* t$ can be defined by

$$\frac{\partial^*}{\partial^* t}\phi \equiv \frac{\partial}{\partial t}\phi + \boldsymbol{u}^* \cdot \boldsymbol{\nabla}\phi. \tag{3}$$

The composite velocity vector is defined as $\boldsymbol{u}^* \equiv \boldsymbol{u} - \boldsymbol{n}S_d$ with $\boldsymbol{n} \equiv \boldsymbol{\nabla}c/|\nabla c|$ being the normal direction of the local isosurface. Using these definitions, Eq. (1) reduces to $\frac{\partial^*}{\partial^* t}c = 0$, reflecting the fact that c remains constant for any point that follows the isosurface.

In a general reacting flow system characterized by Eq. (1), an instantaneous surface-

average of a quantity ϕ conditioned on the isosurface $c(\boldsymbol{x},t)=\hat{c}$ can be defined [8] as

$$\langle\phi\rangle_s|_{\hat{c},t} \equiv \overline{\phi|\nabla c|\delta(c-\hat{c})} \;/\; \overline{|\nabla c|\delta(c-\hat{c})}. \tag{4}$$

Here, $\hat{c}$ is a reference value of the reaction progress variable on an isosurface, $\delta(c-\hat{c})$ is the Dirac delta function and over-line denotes ensemble and volume averages taken simultaneously, i.e., $\overline{\phi} \equiv \lim_{M\to\infty}\frac{1}{M}\sum_{i=1}^{M}\frac{1}{V}\iiint_V \phi_{(i)}(t,\boldsymbol{x})\,\mathrm{d}\boldsymbol{x}$, where M is the number of realizations in the ensemble and $\phi_{(i)}$ pertains to the i-th realization. Note that the Dirac delta function in Eq. (4) can be removed by using the divergence theorem, giving

$$\widehat{A}|_{\hat{c},t}\,\langle\phi\rangle_s|_{\hat{c},t} = \widehat{\oiint_{S|_{\hat{c},t}}\phi\,\mathrm{d}s}. \tag{5}$$

Here, $S|_{\hat{c},t}$ is the isosurface defined by $c(\boldsymbol{x},t)=\hat{c}$ whose total area is equal to $A|_{\hat{c},t}\equiv\oiint_{S|_{\hat{c},t}}\mathrm{d}s$. The long-hat operator over any expression represents the ensemble-averaged value, i.e. $\widehat{\phi}\equiv\lim_{M\to\infty}\frac{1}{M}\sum_{i=1}^{M}\phi_{(i)}$. The rate of change of the total area is related to the stretch rate by $\frac{\partial}{\partial t}A|_{\hat{c},t}=\oiint_{S|_{\hat{c},t}}\mathcal{K}\,\mathrm{d}s$ since the stretch rate, defined as $\mathcal{K}\equiv a_t - S_d\nabla\cdot\boldsymbol{n}$, is well-known [9, 2] to control the rate of change in the area ($\mathrm{d}s$) of an infinitesimal element of an iso-scalar surface, i.e. $\mathcal{K}=\frac{1}{\mathrm{d}s}\frac{\partial^*}{\partial^* t}\mathrm{d}s$. Here, $a_t\equiv\nabla\cdot\boldsymbol{n}-n_in_j(\partial u_i/\partial x_j)$ is the tangential strain rate. The time derivative of Eq. (5) can now be expanded using the chain rule [10] to yield

$$\frac{\partial\langle\phi\rangle_s}{\partial t}+\langle\phi\rangle_s\frac{\partial\widehat{A}}{\partial t}/\widehat{A} = \widehat{\oiint_S\frac{\partial^*\phi}{\partial^* t}\mathrm{d}s}/\widehat{A} + \widehat{\oiint_S\phi\mathcal{K}\,\mathrm{d}s}/\widehat{A}. \tag{6}$$

Eq. (6) can be rewritten to give a general evolution equation for surface-averaged value of the quantity ϕ,

$$\frac{\partial\langle\phi\rangle_s|_{\hat{c},t}}{\partial t} = \left\langle\frac{\partial^*}{\partial^* t}\phi\right\rangle_s|_{\hat{c},t} + \langle\phi\mathcal{K}\rangle_s|_{\hat{c},t} - \langle\phi\rangle_s|_{\hat{c},t}\,\langle\mathcal{K}\rangle_s|_{\hat{c},t}, \tag{7}$$

which holds on all isosurfaces $\hat{c}\in(0,1)$ and time instants and for arbitrary variables ϕ. If ϕ is the displacement speed, S_d, an equation for surface-averaged S_d can then be obtained as long as $\frac{\partial^*}{\partial^* t}S_d$ is known. For this purpose, rewrite Eq. (2) as

$$S_d|\nabla c| = \frac{1}{\rho}\boldsymbol{\nabla}\cdot(\rho\mathcal{D}\boldsymbol{\nabla}c)+\mathbb{W}. \tag{8}$$

Now make the two assumptions that $\rho\mathcal{D}$ =constant and that the reaction rate $\mathbb{W}$ depends solely on c. Apply the operator $\frac{\partial^*}{\partial^* t}$ to Eq. (8) to get

$$\frac{\partial^*}{\partial^* t}S_d = -S_d\frac{\partial^*}{\partial^* t}\ln|\nabla c| + \frac{\mathcal{D}}{|\nabla c|}\frac{\partial^*}{\partial^* t}(\nabla^2 c), \tag{9}$$

because $\frac{\partial^*}{\partial^* t}\mathbb{W}=\frac{\partial\mathbb{W}}{\partial c}\frac{\partial^*}{\partial^* t}c=0$. Finally, substitute Eq. (9) into Eq. (7) with $\phi=S_d$ to get

$$\frac{\partial}{\partial t}\langle S_d\rangle_s|_{\hat{c},t} = \underbrace{-\left\langle S_d\frac{\partial^*}{\partial^* t}\ln|\nabla c|\right\rangle_s|_{\hat{c},t}}_{T_1} + \underbrace{\left\langle\frac{\mathcal{D}}{|\nabla c|}\frac{\partial^*}{\partial^* t}(\nabla^2 c)\right\rangle_s|_{\hat{c},t}}_{T_2} + \underbrace{\langle S_d\mathcal{K}\rangle_s|_{\hat{c},t} - \langle S_d\rangle_s|_{\hat{c},t}\,\langle\mathcal{K}\rangle_s|_{\hat{c},t}}_{T_3}. \tag{10}$$

The temporal evolution in averaged S_d is due to the three terms T_1, T_2 and T_3. The term T_1 is attributed to the isosurface-following rate of change in $|\nabla c|$, or in other words,

decreasing/increasing in the separation distance between neighboring isosurfacees, while term T_2 is due to the isosurface-following rate of change in diffusion. The term T_3 is related to a stretch-rate-induced difference between the averaged isosurface-following derivative and the time derivative of the isosurface-averaged value, i.e. $\frac{\partial}{\partial t}\langle S_d\rangle_s - \left\langle \frac{\partial^*}{\partial^* t} S_d \right\rangle_s$. In Ref. [7] we further showed that T_1 and T_2 can be recast into a form containing only spatial derivatives to facilitate their extraction from numerical simulations:

$$\frac{\partial^*}{\partial^* t}(\nabla^2 c) = -\frac{\partial c}{\partial x_i}\frac{\partial^2 u_i^*}{\partial x_j^2} - 2\frac{\partial^2 c}{\partial x_i \partial x_j}\frac{\partial u_i^*}{\partial x_j} = -\boldsymbol{\nabla} c \cdot \nabla^2 \boldsymbol{u}^* - 2\nabla\nabla c : \nabla \boldsymbol{u}^*, \tag{11}$$

$$\frac{\partial^*}{\partial^* t}\ln|\nabla c| = \mathcal{K} - \nabla_{\bullet}\boldsymbol{u}^*. \tag{12}$$

Finally, Eqs. (11) and (12) can be substituted into Eq. (10) to yield the following fully expanded equation (note: conditioning superscript is dropped for brevity) which is originally given in paper [7] as

$$\begin{aligned}\frac{\partial}{\partial t}\langle S_d\rangle_s = &-\langle S_d \nabla_{\bullet}(S_d\boldsymbol{n})\rangle_s + \langle S_d \nabla_{\bullet}\boldsymbol{u}\rangle_s - \langle S_d\rangle_s\langle\mathcal{K}\rangle_s \\ &- 2\mathcal{D}\left\langle \frac{\nabla\nabla c : \nabla\boldsymbol{u}}{|\nabla c|}\right\rangle_s + \mathcal{D}\left\langle \boldsymbol{n}\cdot\nabla^2(S_d\boldsymbol{n})\right\rangle_s + 2\mathcal{D}\left\langle \frac{\nabla\nabla c : \nabla(S_d\boldsymbol{n})}{|\nabla c|}\right\rangle_s - \mathcal{D}\left\langle \boldsymbol{n}\cdot\nabla^2\boldsymbol{u}\right\rangle_s\end{aligned} \tag{13}$$

Computational setup

The major goal of the present paper is to use the evolution equation for surface-averaged S_d derived above, i.e. Eq. (10), to study highly disturbed turbulent reaction waves. For this purpose, a representative highly turbulent case (case C in the following) is selected from a large DNS database [11–17]. In those DNSs, propagation of a statistically one-dimensional (1D), initially planar, single-reaction wave in a homogeneous, isotropic, statistically stationary forced turbulence was simulated in the case of a dynamically passive wave, i.e. a wave that does not change the fluid density and viscosity and does therefore not affect turbulence. The invoked simplifications allowed us to sample more statistics, as will be discussed later, and to investigate a large number of substantially different cases. Moreover, the simplifications significantly facilitate analysis and interpretation of the DNS data.

While the above derivation of the evolution equation was performed in a simplified, but, more general condition of $\rho\mathcal{D}$=const in which the density is not required to be constant, the equation is mainly kinematic in nature and do not involve terms that are directly associated with thermal expansion effects. Therefore, while thermal expansion plays an important role in premixed turbulent flames, as reviewed elsewhere [18, 19], they seem to be of secondary importance for the derived evolution equation. Accordingly, numerical results reported in the following appear to be relevant not only to constant-density turbulent reacting flows, but also to premixed flames.

DNS database

Since the DNS attributes are discussed in detail elsewhere [11–16], we will restrict ourselves to a brief summary of the simulations. The propagation of a single-reaction wave is governed by the equation

$$\frac{\partial c}{\partial t} + \mathbf{u}\cdot\nabla c = \mathcal{D}\nabla^2 c + W, \tag{14}$$

where

$$W = \frac{1}{1+\tau}\frac{1-c}{\tau_R}\exp\left[-\frac{Ze(1+\tau)^2}{\tau(1+\tau c)}\right] \tag{15}$$

is the reaction rate, τ_R is a constant reaction time scale, $\tau = 6$ and $Ze = 6$ in order for the rate W to depend on c in a highly non-linear manner. Equation (14) is a simplified form of Eq. (1) with $\mathbb{D} = \mathcal{D}\nabla^2 c$ and $\mathbb{W} = W$. The wave propagates in a forced, homogeneous and isotropic turbulence described by the Navier-Stokes equations

$$\frac{\partial \mathbf{u}}{\partial t} + (\mathbf{u}\cdot\boldsymbol{\nabla})\mathbf{u} = -\rho^{-1}\nabla p + \nu\nabla^2\mathbf{u} + \mathbf{f}, \tag{16}$$

where p is the pressure and the density ρ and kinematic viscosity ν are constants, and, therefore, the flow is not affected by wave propagation, as mentioned earlier. A function $\mathbf{f}$ is used to maintain turbulence intensity by applying energy forcing at low wavenumbers [20].

The wave evolves in a rectangular box with size of $\Lambda_x \times \Lambda \times \Lambda$ represented using a uniform grid of $N_x \times N \times N$ cubic cells. The boundary conditions are periodic not only in the transverse directions y and z, but also in direction x normal to the mean wave surface. In other words, when the reaction wave reaches the left boundary ($x = 0$) of the computational domain, the identical reaction wave enters the domain through its right boundary ($x = \Lambda_x$). Such a method allows greatly improved sampling of statistics by simulating many cycles of wave propagation through the computational domain, but the method may only be used in the case of $\rho =$ const and $\nu =$ const and provided that the mean wave brush thickness is smaller than the length of computational domain. These constraints are satisfied in all present simulations.

An initial turbulence field is generated by synthesizing prescribed Fourier waves [21] with an initial rms velocity u_0 and the integral scale $\ell_0 = \Lambda/4$. The initial turbulent Reynolds number $Re_0 = u_0\ell_0/\nu$ can be adjusted by changing the domain width Λ. Subsequently, a non-decaying incompressible turbulent field is obtained by integrating Eq. (16). At the same Re_0, turbulent fields characterized by the same rms velocity $u' \approx u_0$, but different longitudinal integral length scales L_{11} are generated [13] by appropriately adjusting $\mathbf{f}$ using a method by Eswaran and Pope [22]. The governing equations are solved using an in-house DNS solver [23] developed for low Mach number reacting flows.

In the present work, both fully-developed (statistically stationary) and transient reaction waves are studied. Simulations are started from the pre-computed laminar-wave profile of $c_L(\xi)$ initially ($t = 0$) released at $x_0 = \Lambda_x/2$ and the subsequent evolution of the field $c(\mathbf{x}, t)$ is simulated by solving Eq. (14). Sampling of the fully-developed statistics is started when a statistically stationary state has been reached and sampling is done for a duration of at least 50 τ_t^0. In order to study transient turbulent reaction waves, several copies of the same pre-computed laminar-wave profiles $c_L(\xi)$ are simultaneously embedded into the turbulent flow in $\mathcal{M}$ equidistantly separated planar zones centered around $x_m/\Lambda_x = (m - 0.5)/\mathcal{M}$. where m is an integer number ($1 \leq m \leq \mathcal{M} = 15$). Subsequently, evolutions of $\mathcal{M}$ non-interfering transient fields $c_m^t(\mathbf{x}, t)$ are simulated by solving $\mathcal{M}$ independent Eqs. (14). The transient simulations are run over $2\tau_t^0$ before being reset. The flow is then populated by $\mathcal{M}$ new profiles of $c_L(\xi_m)$. The cycle is repeated J times giving an ensemble of $J \times \mathcal{M}$ independent transient waves. Time-dependent statistics for the time interval of $2\tau_t^0$ is then computed by averaging the DNS data over the entire ensemble of $c(\boldsymbol{x}, t)$-fields.

Different cases are set up by combining one of the forced turbulence fields and a reaction waves characterized by a laminar speed S_L and thickness $\delta_F = D/S_L$. The required reaction

Table 1: Three representative DNS cases

Case	$\frac{\Lambda_x}{\Lambda}$	N_x	$\frac{u_0}{S_L}$	$\frac{L_{11}}{\delta_F}$	$\frac{\delta_F}{\Delta x}$	Da	Ka	Pe
A	8	2048	5	5.3	24	1.07	0.94	27
B	1	1048	2	5.3	24	2.67	0.38	10.6
C	8	2048	60	1.2	24	0.02	390	69.5

time scale τ_R in Eq. (15) is found through 1D pre-computations of the laminar wave.

Totally 45 cases characterized by the Damköhler number $Da = \tau_t/\tau_F = 0.01\text{-}24.7$, the Karlovitz number $Ka = \tau_F/\tau_\eta = 0.36\text{-}587$, $u'/S_L = 0.5\text{-}90$, and $L_{11}/\delta_F = 0.39\text{-}12.4$ were simulated, with a few cases being designed to show weak sensitivity of computed results to grid resolution, Λ/L_{11}, etc. [13]. Here, $\tau_F = \delta_F/S_L$ is the wave time scale, $\tau_t = L_{11}/u'$ and $\tau_\eta = (\nu/\bar{\varepsilon})^{1/2}$ are integral and Kolmogorov time scales of the turbulence, respectively, and $\bar{\varepsilon} = 2\nu\overline{S_{ij}S_{ij}}$ with $S_{ij} \equiv (\partial_{x_j}u_i + \partial_{x_i}u_j)/2$ is the dissipation rate averaged over the computational domain and for at least $50\tau_t^0$ after turbulence has evolved into statistical stationarity.

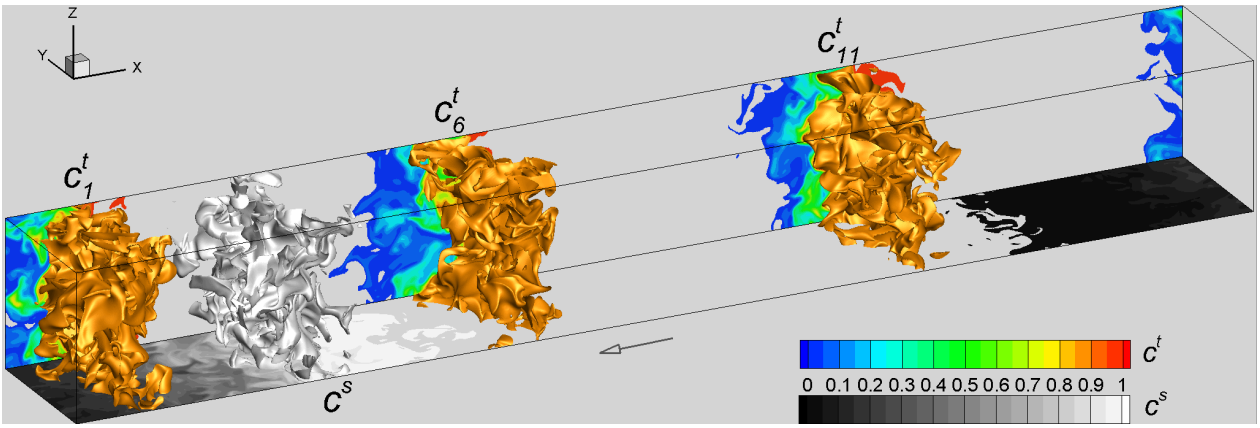

Figure 1: A snapshot of several simultaneously-embedded, non-interfering constant-density reaction waves propagating cyclically on a forced homogeneous turbulence in a fully periodic domain for case C shown in table 1 with Ka=390.

Case setup

In the present paper, the focus is placed on the results obtained in a representative highly turbulent and well resolved case, whose major characteristics are reported in Table 1 (case C), where $Pe = u'L_{11}/\mathcal{D}$ is the turbulent Péclet number and a ratio of $\delta_F/\Delta x$ characterizes the grid resolution in terms on number of grid points per the laminar wave thickness. Moreover, in case C, $L_{11}/\Lambda = 0.11$, $\tau_t^0/\tau_t = 2.3$, and $\eta/\Delta x = 1.1$. Here, $\eta = (\nu^3/\bar{\varepsilon})^{1/4}$ is the Kolmogorov length scale. Figure 1 shows a snapshot with multiple coexisting c^t-fields and one c^s field in case C.

One issue of concern when considering a highly turbulent reaction wave is the appearance of zero-gradient points [24] with $|\nabla c|(\boldsymbol{x}, t) = 0$. Here we should point out that zero gradient points have been excluded from the definitions of surface average in Eq. (4), see [25, 7], however certain quantities of interest, e.g. S_d and $\mathcal{K}$, may locally grow unboundedly large in the neighborhood of a zero-gradient point, which pose a challenge for numerical calculation of surface-averaged quantities. To explore the eventual influence of such points and their

neighborhoods on the accuracy of evaluation of various terms in the evolution equation, two supplementary 2D cases (case A and B) were designed.

Case A is largely identical to case C, but the turbulent field is replaced with a frozen shear flow, i.e. $u(x,y,z,t) = -u_0 \cos(2\pi y/\Lambda)$, $v = w = 0$, and the momentum Eq. (16) is not solved. In case A the isosurfaces are only bent, there is no zero-gradient points in the computational domain. Characteristics of case A, reported in Table 1, are calculated using $L_{11} = \Lambda/2$, $u' = u_0$, and $t_\eta = t_\tau = L_{11}/u_0$.

Case B is designed to have a small number of zero-gradient points in the computational domain. Similarly to case A, case B is also based on a frozen velocity field $u(x,y,z,t) = u''(x,y)$, $v(x,y,z,t) = v''(x,y)$, $w = 0$, and $\boldsymbol{\nabla} \cdot \boldsymbol{u}'' = 0$. The field $\boldsymbol{u}''$ represents a 2D, zero-mean, spatially fluctuating velocity field generated using a reduced version of the method for synthesizing the initial 3D turbulence. Characteristics of case B, reported in Table 1, are calculated by analyzing the 2D velocity field (u_0 and L_{11}) and using $\tau_\eta \approx \tau_t = L_{11}/u_0$ to evaluate Ka. Case B mimics a moderately disturbed reaction wave propagating through vortexes and allowing the appearance of zero-gradient points during collisions of reaction-waves.

Comparison of results computed in cases A (no zero-gradient points), B (a few zero-gradient points), and C (no restrictions on appearance of the zero-gradient points) offers an opportunity to estimate the influence of such points on the accuracy of evaluation of various terms appearing in the S_d-evolution equation.

In the two frozen-velocity cases A and B, simulations of multiple transient waves c^t are performed largely similarly to case C (further details on the difference are discussed in [7]) but the duration of transient sampling is changed from $2\tau_t^0$ to $2\tau_F$.

It is worth noting that the transient data not only are of interest in themselves because the vast majority of premixed turbulent flames are developing flames, as discussed in details elsewhere [26, 27], but also offer an opportunity to control the following numerical issue. As discussed earlier, in very intense turbulence, a scalar isosurface of $c(\boldsymbol{x},t) = \hat{c}$ can become very complicated and can contain multiple zero-gradient points, close to which a quantity ϕ of interest can be unboundedly large. As a result, certain surface-averaged ϕ might be unbounded. Since the transient waves $c_m^t(\boldsymbol{x},t) = \hat{c}$ begin their evolution from a regular flat initial surface, monitoring evolution of (i) isosurfaces of the transient fields $c_m^t(\boldsymbol{x},t) = \hat{c}$ and (ii) the relevant surface-averaged quantities offers an opportunity to detect any anomaly in the developing surface-averaged values of various ϕ and to see eventual influence of the zero-gradient points on various surface-averaged terms in the derived evolution equations.

Result and Discussion

DNS data has been used to examine the evolution equation for surface-averaged S_d, Eq. (10). This equation should hold for all isosurfaces of $c(\boldsymbol{x},t) = \hat{c}$ such that $\hat{c} \in (0,1)$ and at all time instants t. Our emphasis is on contributions to the rate of change in averaged displacement speed due to the three terms T_1, T_2 and T_3.

In each simulated case (A, B, or C), the following terms were computed: (a) the left hand side (lhs) term, i.e. the time derivative of $\langle S_d \rangle_s$, (b) the three rhs terms in Eq. (10), and (c) the sum of all the rhs terms, i.e. $\sum$rhs. Figure 2 shows, for all three cases A-C, the temporal evolution of these terms normalized by the corresponding laminar value, conditioned on three $\hat{c}$ representing the preheat zone $c(\boldsymbol{x},t) = 0.1$, a middle zone $c(\boldsymbol{x},t) = 0.5$ and the reaction zone $c(\boldsymbol{x},t) = 0.88$ where $W(0.88) = \max(W)$.

To match the duration for sampling transient statistics, the time t is normalized by τ_F^* which is set to τ_F in the two cases A and B and τ_t ($\approx \tau_F/22.5$) in the case C. Figure 3 shows

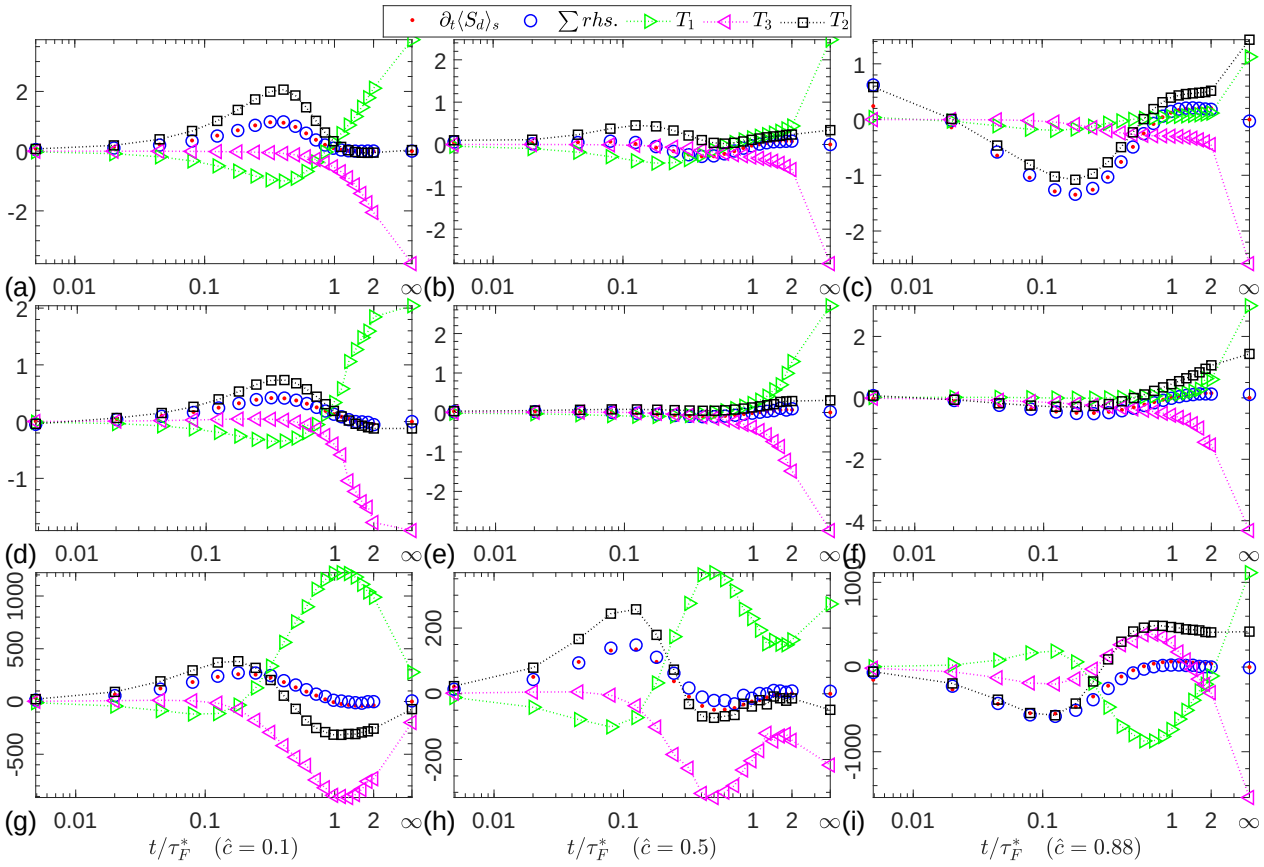

Figure 2: Time dependencies of the lhs term, three individual rhs terms, and sum of all rhs terms from Eq. (10). Results obtained for $\hat{c}$=0.1, $\hat{c}$=0.5 and $\hat{c}=0.88$ are plotted in the left, middle and right columns, respectively. Cases A, B, and C are reported in the top, middle, and bottom rows, respectively. Time is normalized with $\tau_F^*=\tau_F$ in cases A and B or $\tau_F^*=\tau_F/22.5$ in case C. All terms are normalized with S_L/δ_F^2.

the $\hat{c}$-isosurface-dependence of all terms at three representative time instants: an early instant at $0.045\tau_F^*$, a middle instant $1.125\tau_F^*$, and the fully developed state at t_∞. Furthermore, the averaged displacement speed $\langle S_d\rangle_s$ is shown in Fig. 4 at similar conditions as those in Figs. 2 and 3. Note that the lhs term $\frac{\partial}{\partial t}\langle S_d\rangle_s$ (red dots in all the figures) is evaluated by first obtaining the sequence of transient-evolving $\langle S_d\rangle_s$ calculated at 20 sampled time instants of $t_i=(i^2/200)\tau_F^*$ for $i=(1,..,20)$ and then applying a discrete approximation of the time derivative.

Figures 2 and 3 show that the difference between $\frac{\partial}{\partial t}\langle S_d\rangle_s$ and $\sum$rhs is small for all cases A-C for almost all isosurfaces and time instants. This fact supports Eq. (10) and also indicate that all terms have been computed with high enough numerical accuracy.

Before proceeding to discussion of Eq. (10), one may notice in Fig. 4 that averaged displacement speeds are negative in the reaction zone in the high Ka case C during the transient wave evolution. For the fully developed reaction wave in all three cases, the averaged displacement speed recovers to be positive throughout all wave zones and its value stay slightly above unity, see Fig. 4.c. We want to point that high probability of finding negative displacement speed has been reported in previous works [5] studying a fully developed thin reaction zone regime flame which enables heat release and therefore allows density variation,

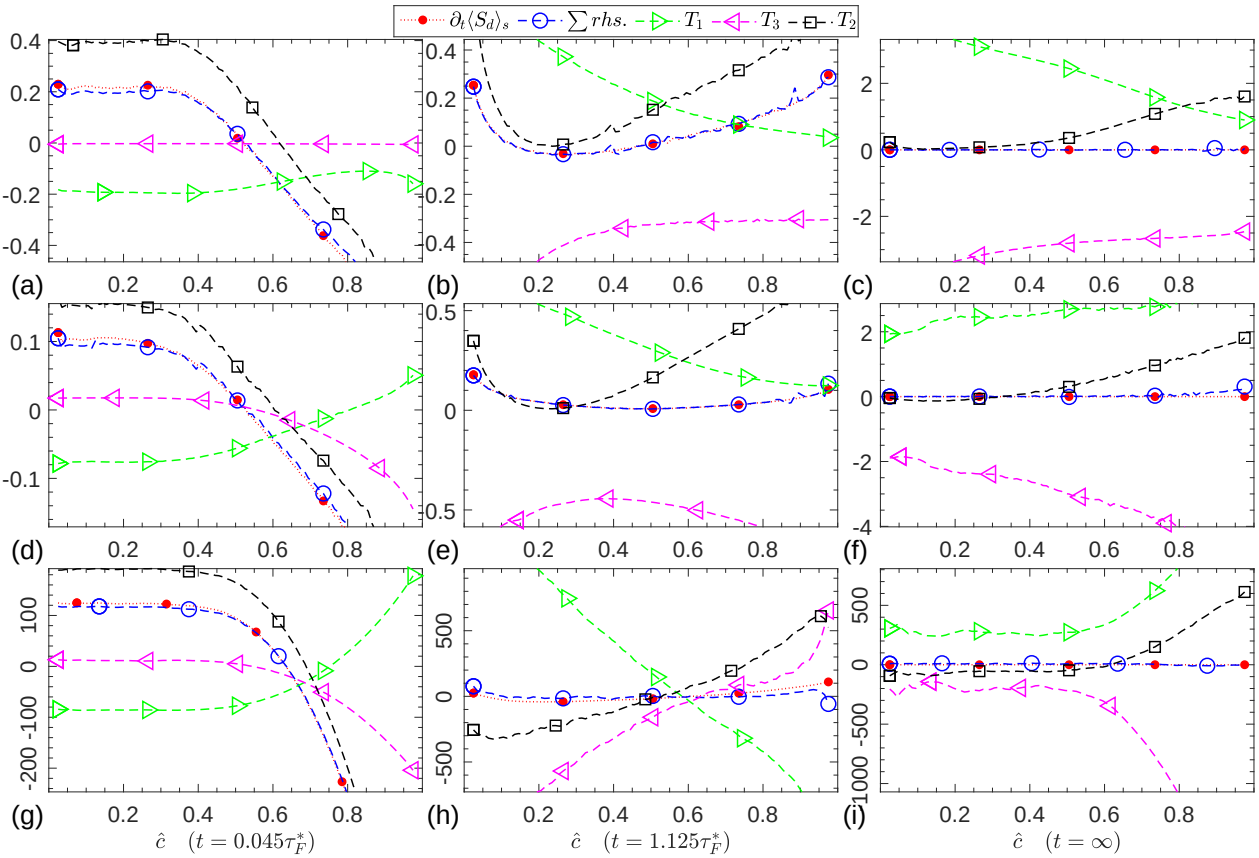

Figure 3: The $\hat{c}$-dependencies of the lhs term, three individual rhs terms, and sum of all rhs terms from Eq. (10). Results computed at $t = 0.045\tau_F^*$ and $t = 1.125\tau_F^*$ are plotted in the left and middle columns, respectively, with $\tau_F^* = \tau_F$ in cases A and B or $\tau_F^* = \tau_F/22.5$ in case C. Results obtained from the fully-developed waves are reported in the right column. Results computed in cases A, B, and C are shown in the top, middle, and bottom rows, respectively. All terms are normalized with S_L/δ_F^2.

however, the averaged displacement speed on this flame was reported to remain positive throughout entire flames.

Trend in fully developed wave

When a reacting wave has evolved into a statistically stationary state, or being fully developed, the time derivative of any statistic must be zero. Therefore, for Eq. (10) at t_∞, the lhs term as well as the sum of all rhs terms must be zero for all $\hat{c} \in (0, 1)$, this is clearly shown for the three cases A, B and C in Figs. 3.c, f and i (blue open circles and red dots). However, each of the three individual rhs terms, T_1, T_2 and T_3, does not necessary need to be zero at t_∞. In fact, Figs. 3.c, f and i show, in the fully developed cases A-C, that T_3 stays negative and T_1 stays positive along all $\hat{c}$. The value of T_2 generally rises with an increase in $\hat{c}$, the value of T_2 at the reaction zone ($\hat{c} > 0.8$) is positive, however in the far upstream preheat zone ($\hat{c} = 0.1$) its value drops slightly below zero when the reaction wave becomes more disturbed by the flow (compare case A and case C). In the two low Ka cases A and B, the maximum absolute value of all three (normalized) terms at t_∞ across all $\hat{c}$ stay below 4; in the high Ka case C this value significantly increases above 1000.

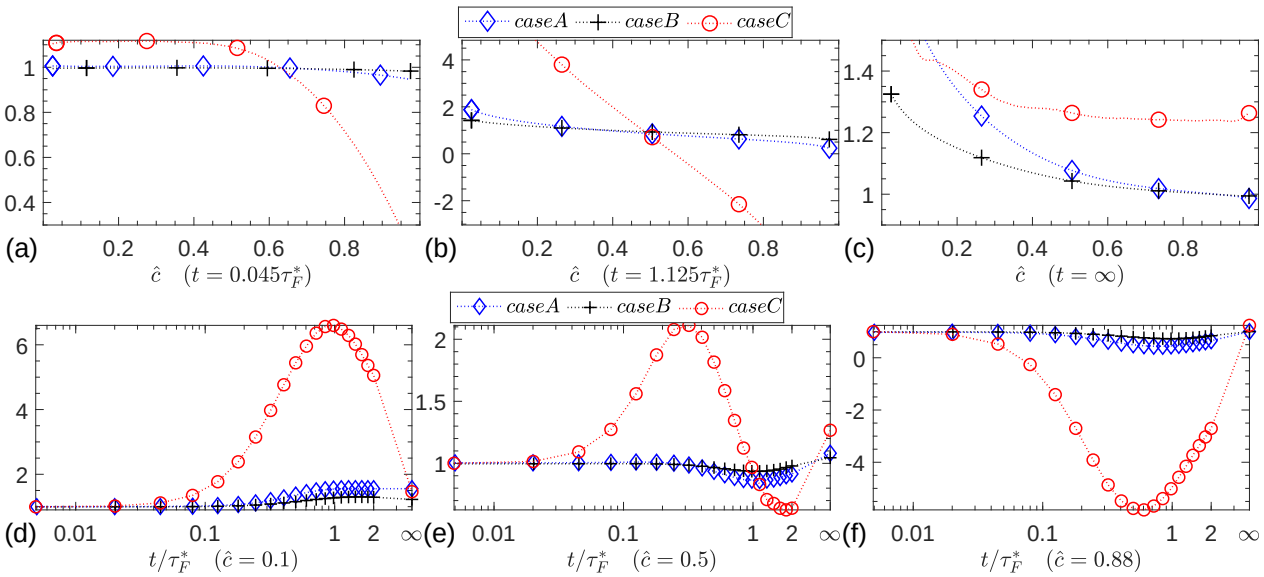

Figure 4: First row: the averaged displacement speed $\langle S_d \rangle_s|_{\hat{c},t}$ plotted against $\hat{c}$ at three representative time instants shown in different columns. Second row: $\langle S_d \rangle_s|_{\hat{c},t}$ plotted against time t at three different $\hat{c}$ shown in different columns. All data from three cases A,B,C is normalized by S_L. Note: $\tau_F^* = \tau_F$ in cases A and B or $\tau_F^* = \tau_F/22.5$ in case C.

Trends during transient wave evolution

For the temporal evolution of terms in Eq. (10) one may notice that the early evolution trend in the time derivative term $\frac{\partial}{\partial t}\langle S_d \rangle_s$ is different in the preheat zone ($\hat{c} = 0.1$) than in the reaction zone ($\hat{c} = 0.88$). In the preheat zone the term $\frac{\partial}{\partial t}\langle S_d \rangle_s$ rises from an initial zero to a positive peak, seen for $0 < t/\tau_F^* \approx 0.3$ in Figs. 2.a and d for cases A and B, as well as for $0 < t/\tau_F^* \approx 0.1$ for case C in Fig. 2.g. On the contrary the term $\frac{\partial}{\partial t}\langle S_d \rangle_s$ in the reaction zone $\hat{c} = 0.88$ drops from an initial zero to a negative peak for the same early duration as shown in Figs. 2.c, f and i. These early trends are further reflected by the negative slope in the profile of $\frac{\partial}{\partial t}\langle S_d \rangle_s$ along $\hat{c}$ shown at a representative early instant $t/\tau_F^* = 0.045$ in Figs. 3.a, d and g. The observed early negative slope in $\frac{\partial}{\partial t}\langle S_d \rangle_s$ is mainly attributed to the diffusion contribution term T_2, compare T_2 with $\partial_t \langle S_d \rangle_s$ in Figs. 2.a, d and g.

In fact, among the three time-dependent terms T_1, T_2 and T_3 shown in Fig. 2, the overall temporal evolution of $\frac{\partial}{\partial t}\langle S_d \rangle_s$ is best mimicked by the diffusion contribution term T_2, even though significant difference between the other two terms always exists at t_∞. The two terms T_1 and T_3 tend to develop values of significant magnitude with opposite sign during later time of wave evolution, compare two curves plotted in triangles both in Fig. 2 for $t/\tau_F^* > 0.3$ and in Fig. 3. Each of the two terms T_1 and T_3 conditioned at the reaction zone ($\hat{c} = 0.88$) can even change its sign twice during its evolution, as shown in Fig. 2.i for the high Ka case C. Such an oscillating behavior is more clearly observed by comparing Figs. 3.g, h and i, which show that the overall slope of the profile T_1 along $\hat{c}$ at three time instants changes from positive to negative and then finally back to positive. Moreover, unlike being a single signed fully-develop $\hat{c}$-profile, each of the terms T_1 and T_3 can change its sign at certain $\hat{c} \approx 0.6-0.7$, see Figs. 3.g and h in high Ka case C at intermediate instants t/τ_F^*=0.045 or 1.25.

One consequence of the above phenomenon is that the maximum magnitude of the variation in all displayed terms during the transient variation conditioned at the middle zone, shown in Fig. 2.h for $\hat{c} = 0.5$, is much smaller than the ones conditioned at the two other

zones, shown in Figs. 2.g and i for $\hat{c} = 0.1$ and $\hat{c} = 0.88$, respectively.

Acknowledgments
RY and TN gratefully acknowledges the financial support by the Swedish Research Council (VR). AL gratefully acknowledges the financial support by CERC and Chalmers Transport Area of Advance. The simulations were performed using the computer facilities provided by the Swedish National Infrastructure for Computing (SNIC) at PDC and HPC2N.

*

References

[1] Williams, F., *Combustion Theory*, CRC Press, 1985.

[2] Candel, S.M., Poinsot, T.J., "Flame Stretch and the Balance Equation for the Flame Area", *Combust. Sci. Technol.* 70:1 (1990).

[3] PETERS, N., *Turbulent combustion*, Cambridge University Press, 2000.

[4] Gran, I.R., Echekki, T., Chen, J.H., "Negative flame speed in an unsteady 2-D premixed flame: A computational study", *Symp. Combust.* (1996).

[5] Chakraborty, N., "Comparison of displacement speed statistics of turbulent premixed flames in the regimes representing combustion in corrugated flamelets and thin reaction zones", *Phys. Fluids* 19:105109 (2007).

[6] Dopazo, C., Martín, J., Hierro, J., "Local geometry of isoscalar surfaces", *Phys. Rev. E* 76:056316 (2007).

[7] Yu, R., Lipatnikov, A.N., "Surface-averaged quantities in turbulent reacting flows and relevant evolution equations", *Submitt. to Phys. fluids* (2019).

[8] Veynante, D., Vervisch, L., "Turbulent combustion modeling", *Prog. Energy Combust. Sci.* 28:193 (2002).

[9] Pope, S.B., "The evolution of surfaces in turbulence", *Int. J. Eng. Sci.* 26:445 (1988).

[10] Grinfeld, P., "Hamiltonian Dynamic Equations for Fluid Films", *Stud. Appl. Math.* 125:223 (2010).

[11] Yu, R., Lipatnikov, A.N., Bai, X.S., "Three-dimensional direct numerical simulation study of conditioned moments associated with front propagation in turbulent flows", *Phys. Fluids* 26:085104 (2014).

[12] Yu, R., Bai, X.S., Lipatnikov, A.N., "A direct numerical simulation study of interface propagation in homogeneous turbulence", *J. Fluid Mech.* 772:127 (2015).

[13] Yu, R., Lipatnikov, A.N., "DNS study of dependence of bulk consumption velocity in a constant-density reacting flow on turbulence and mixture characteristics", *Phys. Fluids* 29:065116 (2017).

[14] Yu, R., Lipatnikov, A.N., "Direct numerical simulation study of statistically stationary propagation of a reaction wave in homogeneous turbulence", *Phys. Rev. E* 95:063101 (2017).

[15] Elperin, T., Kleeorin, N., Liberman, M., Lipatnikov, A., Rogachevskii, I., Yu, R., "Turbulent diffusion of chemically reacting flows: theory and numerical simulations", *Phys. Rev. E* 96:053111 (2016).

[16] Yu, R., Lipatnikov, A.N., "A DNS Study of Sensitivity of Scaling Exponents for Premixed Turbulent Consumption Velocity to Transient Effects", *Flow, Turbul. Combust.* (2018).

[17] Sabelnikov, V.A., Yu, R., Lipatnikov, A.N., "Thin reaction zones in highly turbulent medium", *Int. J. Heat Mass Transf.* 128:1201 (2019).

[18] Lipatnikov, A.N., Chomiak, J., "Effects of premixed flames on turbulence and turbulent scalar transport", (2010).

[19] Sabelnikov, V.A., Lipatnikov, A.N., "Recent Advances in Understanding of Thermal Expansion Effects in Premixed Turbulent Flames", *Annu. Rev. Fluid Mech.* 49:91 (2017).

[20] Lamorgese, A.G., Caughey, D.A., Pope, S.B., "Direct numerical simulation of homogeneous turbulence with hyperviscosity", *Phys. Fluids* 17:015106 (2005).

[21] Yu, R., Bai, X.S., "A fully divergence-free method for generation of inhomogeneous and anisotropic turbulence with large spatial variation", *J. Comput. Phys.* 256:234 (2014).

[22] Eswaran, V., Pope, S.B., "An examination of forcing in direct numerical simulations of turbulence", *Comput. Fluids* 16:257 (1988).

[23] Yu, R., Yu, J., Bai, X.S., "An improved high-order scheme for DNS of low Mach number turbulent reacting flows based on stiff chemistry solver", *J. Comput. Phys.* 231:5504 (2012).

[24] Gibson, C.H., "Fine structure of scalar fields mixed by turbulence. I. Zero-gradient points and minimal gradient surfaces", *Phys. Fluids* 11:2305 (1968).

[25] Yu, R., Lipatnikov, A.N., "Statistics conditioned to iso-scalar surfaces in highly turbulent premixed reacting systems", *Submitt. to Comput. fluids* (2019).

[26] Lipatnikov, A.N., Chomiak, J., "Turbulent flame speed and thickness: Phenomenology, evaluation, and application in multi-dimensional simulations", *Prog. Energy Combust. Sci.* 28:1–74 (2002).

[27] Lipatnikov, A., *Fundamentals of Premixed Turbulent Combustion*, CRC Press, 2012.